

Update of the CLRP Monte Carlo TG-43 parameter database for high-energy brachytherapy sources

Habib Safigholi^{a)}, Marc J. P. Chamberland^{b)}, Randle E. P. Taylor^{c)}, Martin P. Martinov, D. W. O. Rogers^{d)}, and Rowan M. Thomson
Carleton Laboratory for Radiotherapy Physics (CLRP), Dept. of Physics,
Carleton University, Ottawa, Ontario, K1S 5B6

^{a)} Present address, Dept of Radiation Oncology, Lady Davis Institute for Medical Research, Jewish General Hospital, McGill University, Montreal, Quebec, H3T 1E2

^{b)} Present address, Medical Physics, The University of Vermont Medical Center, Burlington, Vermont, 05401

^{c)} Present address, Radformation, New York, NY 10017

^{d)} Corresponding author, email drogers@physics.carleton.ca

Abstract

Purpose: To update and extend version 2 of the Carleton Laboratory for Radiotherapy Physics (CLRP) TG-43 dosimetry database (CLRP_TG43v2) for 33 high-energy (HE, ≥ 50 keV) brachytherapy sources (1 ^{169}Yb , 23 ^{192}Ir , 5 ^{137}Cs , and 4 ^{60}Co) using `egs_brachy`, an open-source EGSnrc application. A comprehensive dataset of TG-43 parameters is compiled, including detailed source descriptions, dose-rate constants, radial dose functions, 1D and 2D anisotropy functions, along-away dose-rate tables, Primary and Scatter Separated (PSS) dose tables, and mean photon energies escaping each source. The database also documents the source models which will be freely distributed with `egs_brachy`.

Acquisition and Validation Methods: Datasets are calculated after a recoding of the source geometries using the `egs++` geometry package and its `egs_brachy` extensions. Air kerma per history is calculated in a $10\times 10\times 0.05$ cm³ voxel located 100 cm from the source along the transverse axis and then corrected for the lateral and thickness dimensions of the scoring voxel to give the air kerma on the central axis at a point 100 cm from the source's mid-point. Full-scatter water phantoms with varying voxel resolutions in cylindrical coordinates are used for dose calculations. Most data (except for ^{60}Co) are based on the assumption of charged particle equilibrium and ignore the potentially large effects of electron transport very close to the source and dose from initial beta particles. These effects are evaluated for four representative sources. For validation, data are compared to those from CLRP_TG43v1 and published data.

Data Format and Access: Data are available at https://physics.carleton.ca/clrp/egs_brachy/seed_database_HDRv2 or <http://doi.org/10.22215/clrp/tg43v2> including in Excel (.xlsx) spreadsheets, and are presented graphically in comparisons to previously published data for each source.

Potential Applications: The CLRP_TG43v2 database has applications in research, dosimetry, and brachytherapy planning. This comprehensive update provides the medical physics community with more precise and in some cases more accurate Monte Carlo (MC) TG-43 dose calculation parameters, as well as fully benchmarked and described source models which are distributed with `egs_brachy`.

Key words: High-energy brachytherapy, CLRP, TG-43 Database, EGSnrc, Monte Carlo `egs_brachy`

Table of contents is for drafting and review purposes only.

Contents

I. Introduction	1
II. Acquisition and Validation Methods	1
II.A. Computational tools and Monte Carlo simulations	1
II.B. TG-43 dosimetry parameters calculations	4
II.C. Effects of electron transport and initial betas	5
II.C.1. Effects on dose-rate constants, Λ	5
II.C.2. Effects on radial dose function, $g(r)$	6
II.C.3. Electron transport effects on the anisotropy function, $F(r, \theta)$	8
II.C.4. Effects of initial beta rays and Auger and internal conversion electrons	10
II.C.5. Summary of electron transport effects	11
II.D. Data additional to TG-43 parameters	12
II.E. Data validation	13
II.F. Trends seen in the data	17
III. Data Format and Access	20
IV. Potential Impact	21
V. Conclusion	21
VI. Acknowledgements	22
References	22

I. Introduction

Presently, brachytherapy dosimetry and planning are often based on the methodology introduced in the 1995 AAPM Task Group No. 43 report, (TG-43)¹ and the single source consensus datasets in its various updates and supplements.²⁻⁸ In 2008, the Carleton Laboratory for Radiotherapy Physics (CLRP) TG-43 dosimetry database was published for 42 low-energy (LE) and high-energy (HE) brachytherapy sources (CLRP_TG43v1)⁹⁻¹¹ using the EGSnrc application `BrachyDose`.¹² These data or source models have been extensively cited in the literature.^{5,6,8,13,14} In 2020, an updated version of the CLRP TG-43 dosimetry parameters (CLRP_TG43v2)¹⁵ for 40 LE LDR brachytherapy sources were calculated utilizing `egs_brachy`,¹⁶ an open source EGSnrc application. This comprehensive CLRP_TG43v2 database for LE sources includes dose-rate constants (DRCs), radial dose functions, 1D and 2D anisotropy functions, along-away dose-rate tables, Primary and Scatter Separated (PSS) dose tables for some sources, and mean energies of photon spectra escaping source encapsulation. The purpose of the present study is to update, extend, and benchmark a comprehensive TG-43 dosimetry database for HE brachytherapy sources using a single consistent method using `egs_brachy`. The HE source geometry models were coded using the `egs++` geometry package¹⁷ and systematically reviewed and improved as needed. As of July 2022, twenty new HE sources are added to those in CLRP_TG43v1. Overall, the updated CLRP_TG43v2 datasets include 40 LE and 33 HE sources (1 ¹⁶⁹Yb, 23 ¹⁹²Ir, 5 ¹³⁷Cs, and 4 ⁶⁰Co) compared to the 2008 CLRP_TG43v1 which includes datasets for 27 LE and 15 HE sources.

II. Acquisition and Validation Methods

II.A. Computational tools and Monte Carlo simulations

All Monte Carlo (MC) calculations are performed with the EGSnrc application `egs_brachy`¹⁶ (GitHub commit hash 8166234, 2020, with some source models updated since 2020; available at https://github.com/clrp-code/egs_brachy). `egs_brachy` is benchmarked and documented in previous publications.^{15,16,18} Generally, transport parameters are EGSnrc defaults,¹⁹ using the HE default specifications distributed with `egs_brachy`. As discussed below, electron transport is not generally modelled for ¹⁶⁹Yb, ¹⁹²Ir, and ¹³⁷Cs sources since charged particle equilibrium^{7,10,20} is established not far from the sources and scoring kerma

with the tracklength (TL) estimator is much more efficient.¹⁶ For example, the TL estimator is more efficient by factors of 200 for ^{60}Co and 700 for ^{192}Ir than using energy deposition scoring.

For ^{60}Co sources, electrons are tracked and dose is scored using both energy deposition scoring and the TL kerma estimator. The electron cutoff energy is set to 10 keV as recommended in the literature.^{7,20} Calculations for representative sources [*viz.*, ^{169}Yb (4140), ^{192}Ir (Generic and mHDR-v2), ^{137}Cs (CSM11), and ^{60}Co (all 4 models)] are done with and without electron transport (energy deposition versus TL scoring) to establish if there are differences for DRC, radial dose, and anisotropy functions. The global photon energy transport cutoff (PCUT) is set to 1 keV, except for air-kerma strength calculations for which the cutoff is 10 keV for ^{169}Yb , ^{192}Ir , ^{137}Cs , and ^{60}Co sources as recommended by the AAPM HEBD report.⁷ The 10 keV energy cutoff eliminates the contribution of low-energy characteristic x rays from HE source encapsulations.⁷ For three representative sources [*viz.*, ^{169}Yb (4140), LDR ^{192}Ir (Best), and HDR ^{192}Ir (Generic)] the effect of using a 1 keV cutoff energy on air-kerma strength and DRC values is evaluated. Reducing PCUT from 10 to 1 keV does not change significantly ($\leq 0.1\%$) the values of S_K and DRC for the two ^{192}Ir sources tested. However, for the ^{169}Yb source the corresponding S_K and hence DRC values change significantly (2.8% and -2.8%). The S_K value is increased due to the inclusion of the low-energy photons which are not attenuated in the vacuum while the dose in-phantom at the reference point is not affected by these low-energy photons which are absorbed in the water with a mean-free path of 2 mm or less. The results presented below (Table 2) are for the recommended PCUT=10 keV value although the values for PCUT=1 keV are included in a footnote for the ^{169}Yb source.

Photoelectric absorption, Rayleigh scattering, Compton scattering, and fluorescent emission of characteristic x rays are simulated. Dose is approximated as collision kerma, scored with a TL estimator in voxels with mass energy absorption coefficients (distributed with `egs_brachy`; calculated with EGSnrc application `g` before 2017). Recent improvements in the `g` application²¹ showed that these mass energy absorption coefficient values would change by up to a maximum of 0.2% using the updated release of EGSnrc. Photon cross sections are from the XCOM database.²² The ‘un-renormalized’ photoelectric cross sections are used as opposed to the renormalized cross sections.²³ The energy-fluence-weighted spectrum averaged values of $(\overline{\mu_{\text{en}}}/\rho)$ are proportional to the collision kerma. Calculations of these $(\overline{\mu_{\text{en}}}/\rho)$ values done with either the normalized or unrenormalized cross sections showed differences

of less than 0.02%, 0.03%, 0.02% and 1.0% for the spectra in-air or in-phantom at 1 cm for ^{60}Co , ^{137}Cs , ^{192}Ir , and ^{169}Yb sources respectively. This difference is only an issue for the ^{169}Yb source and even there, the change for the in-air spectrum vs for the in-phantom spectrum differ by about 0.4% so that the effect on the calculated dose-rate constant would be about 0.4%. The uncertainty related to cross section uncertainties on other in-phantom ratio quantities such as $g(r)$ and $F(r, \theta)$ is expected to be even less.

While some issues related to type B uncertainties on the Monte Carlo results have been addressed, *e.g.*, the effects of electron transport, the effects of the selection of the low-energy cutoff, δ , the effects of phantom size or uncertainties related to renormalized vs un-renormalized photoelectric cross sections, the general issue of overall uncertainties has not been addressed here. These have been addressed in the past by TG138.²⁴ Their estimates of the overall $k = 1$ uncertainties on the Monte Carlo calculated values of individual high-energy TG-43 parameters such as the DRC, $g(r)$ and $F(r, \theta)$ were 2.1%, 0.5% and 0.6% respectively.

Initial photon energies are sampled from the NNDC²⁵ spectra which are distributed with the `egs_brachy` package, and also consistent with the HEBD report.^{7,8} Dose calculations are performed with the source located at the center of a full scattering⁷ cylindrical water phantom (80 cm long, 40 cm radius, $\rho = 0.998 \text{ g/cm}^3$). Since sources are cylindrically symmetric, for efficiency purposes, collision kerma and hence absorbed dose are scored in concentric cylindrical shells. To increase efficiency and also minimize bin-size artifacts,¹² the radial and depth resolutions of the cylindrical shells are 0.1 mm for $r \leq 1 \text{ cm}$, 0.5 mm for $1 \text{ cm} < r \leq 5 \text{ cm}$, 1 mm for $5 \text{ cm} < r \leq 10 \text{ cm}$, and 2 mm for $10 \text{ cm} < r \leq 20 \text{ cm}$ where r is the radial distance from the source's central axis. The magnitude of the voxel size effects was discussed previously^{12,26} and is typically $\leq 0.25\%$.¹²

Air-kerma per history is always calculated using a TL estimator for photons above the threshold δ (10 keV normally) in a $10 \times 10 \times 0.05 \text{ cm}^3$ air voxel located effectively in vacuo on the transverse axis 100 cm away from the source and then corrected using $k_{r,2} = 1.00217$ for the lateral and thickness dimensions of the scoring voxel to give the air kerma per history on the central axis at a point 100 cm from the source's mid-point. Although the $k_{r,2}$ formula used here and previously¹² is wrong in general, it has been shown to be highly accurate for the thin detector used here (see ref²⁷ for details) and so is used here. From this, the air-kerma strength per history factor, S_K^{hist} , in $\text{Gy} \cdot \text{cm}^2 / \text{hist}$, is calculated by multiplying the air kerma on axis per history by d^2 , where $d = 100 \text{ cm}$ in this case. This factor is useful

when calculating clinical doses and the DRC, Λ , which is given by

$$\Lambda = \frac{D(1 \text{ cm}, 90^\circ)/\text{hist}}{S_K^{\text{hist}}}, \quad \left[\frac{\text{Gy}/\text{hist}}{\text{Gy}\cdot\text{cm}^2/\text{hist}} \right] = [\text{cm}^{-2}] \equiv [\text{cGy per hour per U}] \quad (1)$$

where $D(1 \text{ cm}, 90^\circ)/\text{hist}$ is the dose to water per history calculated at the reference point at $(1 \text{ cm}, 90^\circ)$. Air kerma is defined in dry air and hence the geometry of the detector's sensitive region for air-kerma calculations is filled with dry air as recommended by TG-43U1S2.⁵

For those phantom voxels which overlapped with the source boundary, dose is scored only in the portion of the voxel which is not occupied by the source and 10^9 or 10^{10} random points per cm^3 are used to determine the volume correction.¹⁵ The number of photon histories generated in each simulation was $\sim 5 \times 10^{10}$ to ensure that results for DRC, $g(r)$, and $F(r, \theta)$ (for angular points away from the source's axis) have $k=1$ statistical uncertainties less than 0.02%, 0.02%, and 0.1% respectively. The uncertainty on $F(r, \theta)$ for the small voxels very close to the source axis can be up to 4.0%.

II.B. TG-43 dosimetry parameters calculations

TG-43 dosimetry parameters^{1,2} *viz.*, radial dose function, $g_L(r)$, 1D anisotropy function (anisotropy factor), $\phi_{an}(r)$, 2D anisotropy function, $F(r, \theta)$, air-kerma strength, S_K , and dose rate constant, DRC or Λ , for 33 HE brachytherapy sources are calculated using methods described in our previous work.^{9,15,28} The only significant difference is the inclusion of data to 20 cm radius compared to 10 cm for the LE database.¹⁵

The 20 new HE sources added to the CLRP_TG43v2 database are shown in Figure 1. A detailed description of all 33 sources is available online in the database.

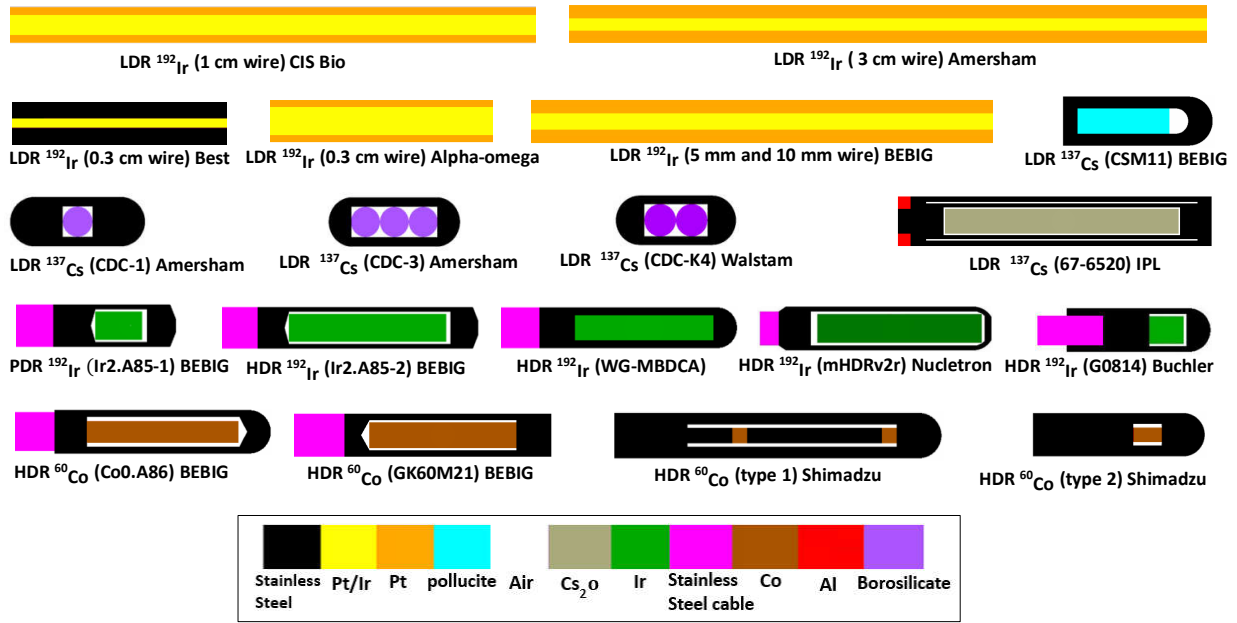


Figure 1: Schematics of the 20 HE brachytherapy sources added to CLRP_TG43v2(the BEBIG ¹⁹²Ir LDR source comes in 2 lengths). Source geometries are generated by egs_view, the EGSnrc viewer. Different sources have different scales, but each source's dimensions are individually to scale.

II.C. Effects of electron transport and initial betas

II.C.1. Effects on dose-rate constants, Λ

The DRCs calculated with electron transport tend to be larger for the higher-energy sources since the electrons transport the energy away from the source in the phantom, thus increasing the dose at the reference point. At the same time electron transport has no effect on the air-kerma strength since the air kerma is typically measured using calibrated ion chambers which are only sensitive to the photon fluence. Hence the calculated air-kerma strength per history factor does not involve transport of electrons from the source. Specific examples of differences in dose-rate constants calculated with and without electron transport in the water phantom are given below in section II.F. and in the footnotes in Tables 1 and 2.

However there is another issue which appears to be overlooked or ignored in the literature *viz.*, the distinction between air collision kerma and air kerma. Whereas measured values are all of air kerma, as far as we can determine (many papers lack sufficient information) calculations are all of air collision kerma based on using $(\mu_{en}/\rho)_{air}$ values integrated over

the photon energy fluence spectrum in the region of interest. For low-energy brachy sources this is completely acceptable. For high-energy sources, using the EGSnrc application *g*,²⁹ the calculated ratios of $(\mu_{\text{tr}}/\rho)_{\text{air}} / (\mu_{\text{en}}/\rho)_{\text{air}}$ averaged over the photon energy-fluence spectra from sources are unity within 0.02%, 0.04%, 0.1%, 0.17% and 0.33% for in-vacuum spectra at 100 cm from representative ^{125}I , ^{169}Yb , ^{192}Ir , ^{137}Cs , and ^{60}Co sources respectively. In principle, the calculated air-kerma strength should be increased by these amounts and hence the dose-rate constants decreased by these amounts. This is only possibly significant for ^{137}Cs and ^{60}Co sources. Nevertheless, in keeping with what appears to be all previous practice, these corrections have not been applied to dose-rate constant values in the database.

II.C.2. Effects on radial dose function, $g(r)$

There have been a variety of studies which look at the effects of electron transport and initial source beta decays on TG-43 parameters.^{10,20,30-32} To show the potential effects of using the tracklength estimator, calculations including electron transport have been done for representative sources with each radionuclide. Fig. 2 shows two $g(r)$ curves for each of four representative sources, one calculated with the TL estimator based only on photon transport and the other using interaction scoring which scores the energy deposited by electrons along their path. The most dramatic effects occur within the first few mm (up to 9 mm for ^{60}Co). Perhaps the most surprising result is the very high value very close to the source for the ^{169}Yb source which has a mean photon energy of only 110 keV. However, there are some photons up to 300 keV and the corresponding electrons escaping from the source deliver considerable dose in the first 0.5 mm. For the higher-energy sources there are clearly buildup effects in play so that even the electrons escaping from the source's cladding have not reached full buildup. Once full buildup is achieved, the electron transport causes a significant bump in the dose to values greater than those from the TL estimator at the same radius (7%, 3%, and 6% for the ^{192}Ir , ^{137}Cs , and ^{60}Co sources here respectively). In external photon beams, the dose does not exhibit a bump relative to the collision kerma. For these brachytherapy sources the bump is due to the multiple scattering of electrons in a radial geometry as demonstrated in Fig. 3 for a ^{60}Co point source. The residual small peak in the no-scatter case is due to the downstream transport of energy before being deposited. This affects the ratio for the entire curve but is maximal at the small radii where the $1/r^2$ drop off in dose is more rapid (see further discussion below). The curve with a high ECUT during the interaction scoring has a value of 1.003 because it is scoring the total kerma rather than the collision kerma scored

by the TL estimator (see section II.C.1.).

Another noteworthy feature of the $g(r)$ curves in Fig. 2 is that the ^{60}Co TL-scored values past 1 cm are slightly greater than the interaction-scored values. This is the reverse of the situation in an external beam.²¹ However, this is an artifact because of the normalization at 1 cm where the interaction-scored value is greater than the TL-scored value. Fig. 4 demonstrates this explicitly.

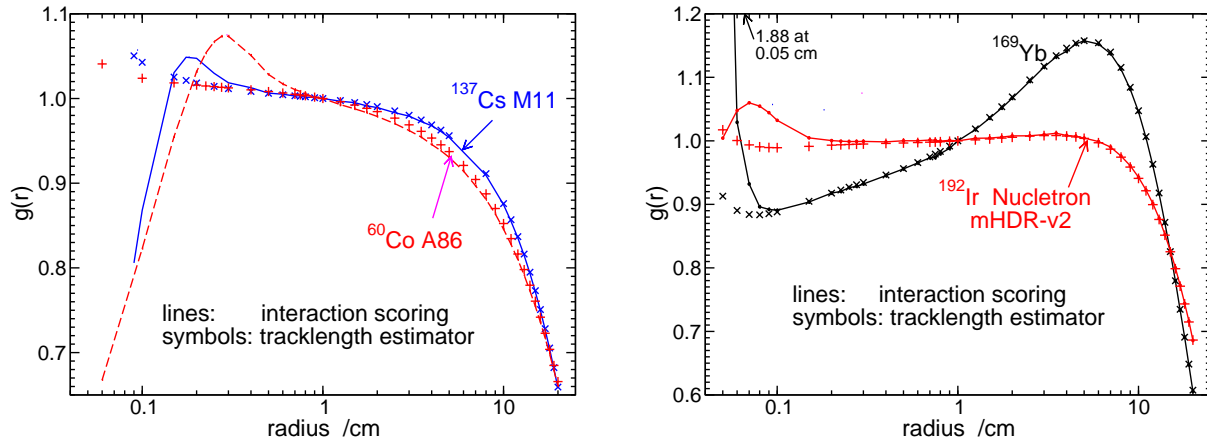


Figure 2: $g(r)$ values for 4 representative high-energy sources with different radionuclides. The line curves (dashed or solid) are calculated scoring energy deposited by electrons created by photon interactions and the symbols (x or +) by the TL estimator which ignores electron transport effects. No beta particles are modelled from the sources.

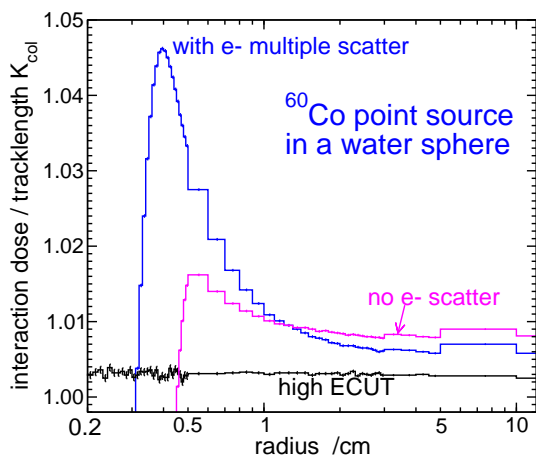


Figure 3: Ratio of dose scored with electron transport to the collision kerma scored with a TL estimator as a function of radius for a point source of 1.25 MeV photons in a sphere of water. The upper curve includes the multiple scatter of the electrons set in motion. The curve with the lower peak has electron scatter turned off. The lowest curve suppressed all electron transport and deposited the electron energy where created.

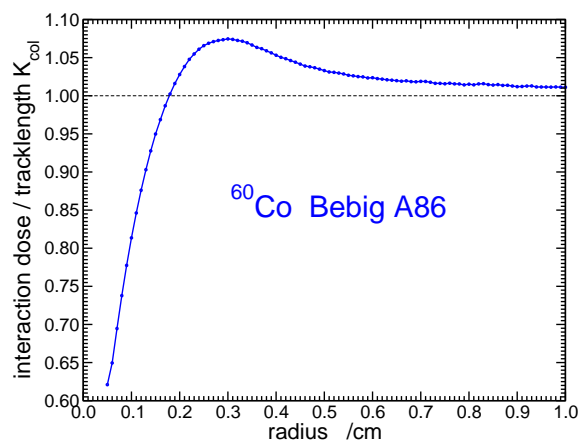


Figure 4: Ratio of the interaction-scored dose to the TL-scored dose radially on the transverse axis of the Bebig A86 ^{60}Co source.

II.C.3. Electron transport effects on the anisotropy function, $F(r, \theta)$

For radii close to the source capsule of the Bebig A86 ^{60}Co source (in this case, at $r=0.26$ cm), Fig. 5 shows that including electron transport plays a significant role in the anisotropy function, $F(r, \theta)$. The HES curves (High E CUT in Source), which suppress electrons coming from the source, show that electrons from the source play an important role when electron transport is accounted for but have virtually no effect when TL scoring is used. The significant drop in the $F(r, \theta)$ values with electron transport compared to that evaluated with the TL estimators for low and high angles is because at these angles the water at radius 0.26 cm is only 0.01 cm from the encapsulation. Hence the electron buildup is not complete as seen in the $g(r)$ curves in Fig. 2 for radii close to the encapsulation. In contrast, at 90° the dose at a radius of 0.26 cm is 0.21 cm from the encapsulation and the dose calculated with electron transport is even higher than that scored with the TL estimator. Hence the drop in the electron transport value of $F(r, \theta)$ for θ away from 90° relative to the TL value is result of the numerator, $D(r, \theta)$, decreasing and the denominator, $D(r, 90^\circ)$, increasing. The right panel of Fig. 5 shows that even at a radius of 0.5 cm there is a small but distinct

effect from considering electron transport.

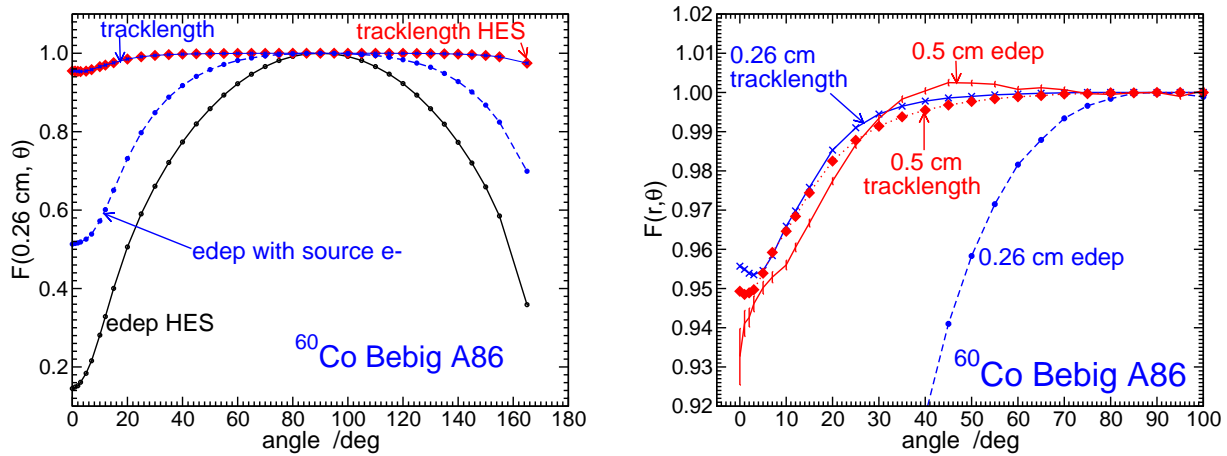


Figure 5: Calculated $F(r, \theta)$ values for the Bebig A86 ^{60}Co source. Left panel: all curves are at $r=0.26 \text{ cm}$. edep means electrons transported and energy deposition scored. HES means “High ECUT in Source capsule” so no electrons escape the capsule. “tracklength” means the TL estimator is used and only scores the photons. Right panel shows the detail from 0 to 100° for radii of 0.26 and 0.5 cm. The source extends 0.25 cm longitudinally and 0.05 cm radially from the mid-point of the active layer.

Fig. 6 shows that for the MBDCA Generic ^{192}Ir source³³ the differences between the two scoring approaches is much less than those for the ^{60}Co source although for small radii close to the ends of the source there are still significant differences which are completely gone by a radius of 1 cm.

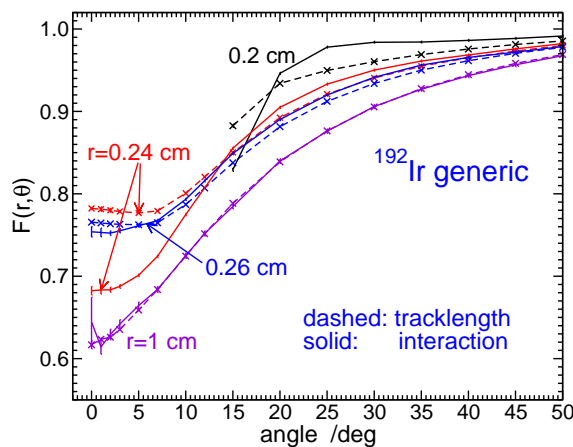


Figure 6: Calculated $F(r, \theta)$ values at different radii for the MBDCA Generic ^{192}Ir source using both interaction scoring and the TL estimator. This source extends 0.235 cm longitudinally from the mid-point of the radioactivity.

Fig. 7 demonstrates that even for the relatively low-energy ^{169}Yb source, the effects of electron transport can be significant at locations near the ends of the source, just as the

effect on the $g(r)$ curve seen in Fig. 2 was significant at radii of less than a mm. The high values for the $r=0.24$ cm curve close to 0° may reflect slight problems related to interpolating for values right at the boundary of the seed.

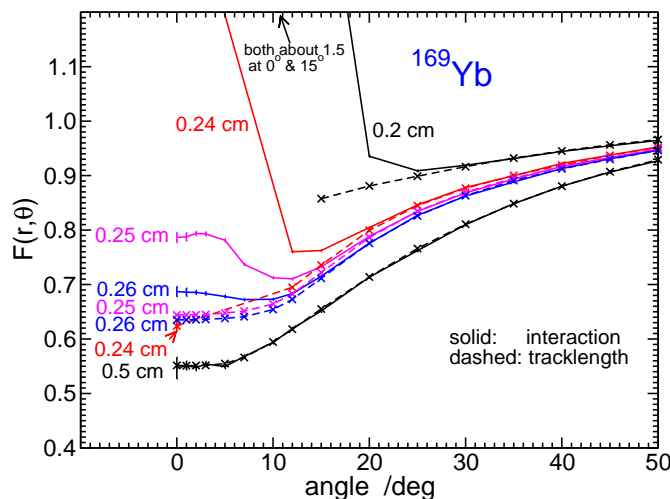


Figure 7: Calculated $F(r, \theta)$ values for the 4140 ^{169}Yb source using both interaction scoring and the TL estimator. This source extends longitudinally 0.24 cm from the mid-point of the radioactivity.

II.C.4. Effects of initial beta rays and Auger and internal conversion electrons

In addition to the dose from photons, there are dose contributions from the betas originating from the radioactive decay and from any Auger electrons from the relaxation of the daughter atom (*e.g.*, 0.082 Auger electrons per disintegration, mostly <6 keV for ^{137}Cs) and any internal conversion electrons from the relaxation of the daughter nucleus (*e.g.*, 0.095 internal conversion electrons per disintegration with energies from 624 to 661 keV for ^{137}Cs).²⁵ Fig. 8 shows the relative dose contribution from these betas around two ^{192}Ir , one ^{137}Cs , and one ^{60}Co source. In addition for the ^{137}Cs source, it shows the relative dose contribution from the internal conversion and Auger electrons. The highest dose contributions come from the betas that escape the source encapsulation. As seen from the results for the 2 different ^{192}Ir sources, the size and extent of this component depends critically on the geometry of the source. For the very thin VariSource ($r=0.295$ mm), the beta dose is much greater than that for the 69% thicker MBDCA Generic ^{192}Ir source ($r=0.5$ mm) and extends farther from the VariSource since many more betas escape the source. Nonetheless, even for the very thin source this component is negligible by 2 mm from the central axis. Past that point there is

a fairly constant component due to bremsstrahlung photons created by the betas. For both ^{192}Ir sources this constant component is about 0.2% of the dose from the initial photons and even less for the ^{137}Cs and ^{60}Co sources, consistent with earlier estimates.^{20,30} The peak dose from betas in the ^{60}Co source is slightly less than from the other sources but extends much farther radially although it is less than 0.2% of the photon dose by a radius of 3 mm. The surprising aspect of this result is that the increased dose is almost entirely due to the 0.12% beta branch which has an endpoint energy of 1491 keV vs the dominant decay with an endpoint energy of 317 keV.

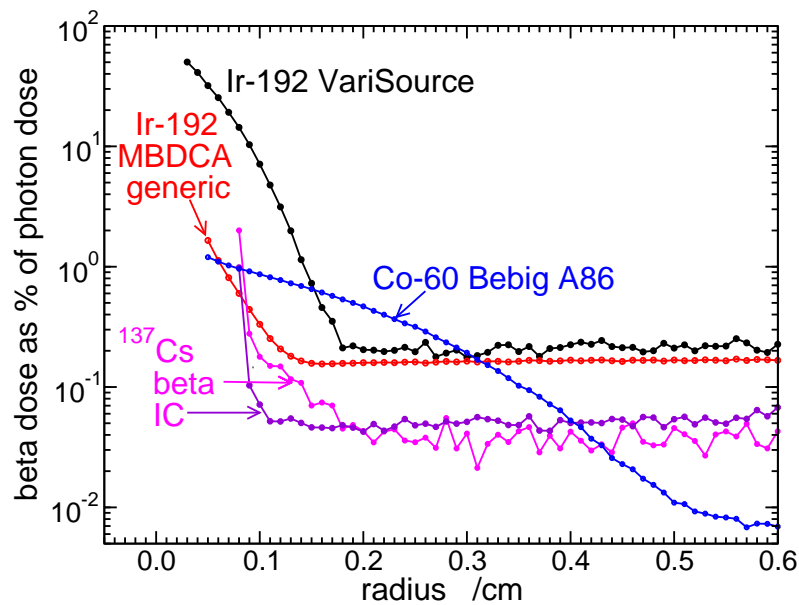


Figure 8: The dose on the transverse axis due to initial electrons as a % of photon dose for 4 sources. The ^{192}Ir beta spectrum is from ref³⁴ as tabulated in ref,³⁵ the ^{60}Co spectrum from ref³⁶ and the other sources from ref.³⁷ There are 2.36 and 2.0 photons per beta decay in the ^{192}Ir and ^{60}Co sources respectively. Internal conversion(IC) and Auger electrons are not considered for these 2 radionuclides. For the ^{137}Cs source there are 0.929 photons and 0.177 internal conversion or Auger electrons per beta decay.²⁵

The present results for the effects of betas and other decay products are generally consistent with the various previous studies mentioned above^{10,20,30-32} given the clear dependence on the geometries of the sources involved.

II.C.5. Summary of electron transport effects

Figures 2 to 8 in this section (II.C.) show significant dosimetric effects for the four different radionuclide sources when tracking electrons before scoring energy deposition and when accounting for the dose due to initial radiations other than photons. However, these effects

are negligible past a radius of 2 mm for the ^{169}Yb and ^{192}Ir sources or past 3 mm for the ^{137}Cs sources. The regions very close to the sources are in the high-dose regions and the accuracy of the calculations there are not clinically important (now that intravascular brachytherapy is no longer common). In the case of ^{60}Co sources the effect spreads out as far as 6 or 7 mm (see Fig. 4) and potentially are clinically relevant. Thus the calculations for the ^{60}Co sources in the database are all reported taking into account electron transport effects although the 1 or 2% effects from the initial betas out to 3 mm radius are not included.

II.D. Data additional to TG-43 parameters

For all HE sources, along and away dose-rate data normalized to the air-kerma strength, S_K , are tabulated in $\text{cGy h}^{-1} \text{U}^{-1}$ at 16 away distances from 0 to 20 cm and 29 along points from -20 to 20 cm. The away data are only needed for values greater than zero due to the cylindrical symmetry of the sources. Primary and Scatter Separated (PSS)¹⁰ dose data are provided. These data include total, primary, single scatter and multiple scatter in polar coordinates. They are normalized to the total photon energy escaping from the source capsule and tabulated at 12 radii from 0.30 to 20 cm and 47 polar angles with resolution of 5° or better. High resolution ($\Delta r = 1 \text{ mm}$, $\Delta \theta = 1^\circ$) PSS data are also provided. For the purpose of these calculations, any photon escaping the source encapsulation is considered a primary photon, only photons which scatter within the phantom are counted in the scatter tallies. In Tables 1 and 2 the mean energy of photons escaping the source surface are provided in column 1 (in brackets). Calculated photon fluences as a function of energy have statistical uncertainties less than 0.2%.

II.E. Data validation

For validation, TG-43 dosimetry parameters are compared to data in the literature. DRC values and their statistical uncertainties are compared to the values computed with **BrachyDose** in the **CLRP_TG43v1**⁹⁻¹¹ database, as well as MC data by other authors cited in Tables 1 and 2. It should be emphasized that although **egs_brachy** and **BrachyDose** are based on EGSnrc, the coding of the geometries is based on completely different geometry packages and hence the comparison is a validation of the geometry models. The comparisons give percent differences as:

$$\% \Delta(\Lambda_1, \Lambda_2) = \frac{\Lambda_1 - \Lambda_2}{\Lambda_1} \times 100\%. \quad (2)$$

DRC values separated by radionuclide are shown in Table 1 and 2 and Figure 9. Due to the large amount of data generated in this work, detailed comparisons of $g(r)$ and $F(r, \theta)$ are omitted here, but the comparisons are available in the database whenever other data are available.

Overall, the CLRPv2 DRC values show good agreement with the available **BrachyDose** data with a maximum difference of 0.6% from the **CLRP_TG43v1**⁹⁻¹¹ database. The average difference between **CLRP_TG43v1** and ‘v2’ for twelve sources is $(-0.19 \pm 0.24)\%$ which is excellent agreement considering the statistical uncertainty of 0.3% on the **BrachyDose** results.⁹⁻¹¹ This excludes the DRC values for two HDR ¹⁹²Ir sources (Flexisource and MicroSelectron-v2) where some small geometry changes were found necessary and explained in each source’s webpage. The resulting changes in the DRC values (-0.53%, and 0.0%) were less than the maximum 0.6% difference between the two databases.

Table 1: Dose-rate constant values for ^{192}Ir sources, calculated by `egs_brachy` ('This work'), `BrachyDose` ('TR'),^{10,38} other codes ('Other MC'), and TG-229's TG-43 consensus data⁸ (TG43_{con}). All `egs_brachy` and `BrachyDose` values are without electron transport. Statistical uncertainties are $\leq 0.3\%$ (BD), $\leq 0.02\%$ (eb), and otherwise shown in brackets (uncertainty in last digit). Percent differences are given between results for `egs_brachy` and the best `BrachyDose` geometry [$\% \Delta(\text{eb}, \text{BD})$], as well as with TG43_{con} [$\% \Delta(\text{eb}, \text{TG43}_{\text{con}})$]. The mean emitted photon energy (\bar{E}_γ) on the surface of each source determined by `egs_brachy` is indicated. Sources are numbered for reference in later figures. Webpages often report several other MC results.

Source model ($\bar{E}_\gamma/\text{keV}$)	Dose-rate constant, DRC or Λ ($\text{cGy h}^{-1} \text{U}^{-1}$)					
	This work(eb)	TR ^{10,38} BD	$\% \Delta$ (eb,BD)	Other MC	TG43_{con} ⁸	$\% \Delta$ (eb, TG43_{con})
^{192}Ir LDR						
1 Amersham, 3 cm wire(358.4)	0.7245	-	-	0.724 ³⁹	-	-
2 CIS Bio, 1 cm wire(360.9)	1.0343	-	-	1.047 ⁴⁰	-	-
3 BEBIG, 1 cm wire(358.1)	1.0362	-	-	1.036(2) ⁴¹	1.036(2)	0.0
4 BEBIG, 0.5 cm wire(358.2)	1.0974	-	-	1.096(2) ⁴¹	1.096(2)	0.1
5 Best, 0.3 cm wire(355.4)	1.1149	-	-	1.112(1) ⁴²	1.110(15)	0.4
6 Alpha-Omega, 0.3 cm wire(360.7)	1.1115	-	-	1.111(1) ⁴²	-	-
^{192}Ir PDR						
7 BEBIG, Ir2.A85-1(361.2)	1.1222	-	-	1.124(11) ⁴³	1.124(1)	-0.2
8 Nucletron, mPDR-v1(359.3)	1.1223	1.119	0.3	1.121(6) ⁴⁴	1.120(6)	0.2
9 Varian, GammaMed 12i(359.0)	1.1239	1.125	-0.1	1.122(3) ⁴⁵	1.126(3)	-0.2
10 Varian, GammaMed Plus(359.0)	1.1242	1.125	-0.1	1.122(3) ⁴⁵	1.123(3)	0.1
^{192}Ir HDR						
11 Generic, WG-MBDCA(360.6)	1.1102 ^a	-	-	1.111(4) ^{33b}	-	-
12 Buchler, G0814(362.3)	1.1211	1.119	0.2	1.115(3) ⁴⁶	1.117(4)	0.4
13 BEBIG, Ir2.A85-2(360.5)	1.1102	-	-	1.109(11) ⁴³	1.109(12)	0.1
14 BEBIG, GI192M11(360.5)	1.1099	1.112	-0.2	1.108(3) ⁴⁷	1.110(4)	0.0
15 Nucletron, Flexisource(360.4)	1.1101 ^c	1.116	-0.5	1.109(11) ⁴⁸	1.113(11)	-0.3
16 Nucletron, mHDR-v1(360.6)	1.1099	1.117	-0.6	1.115(6) ⁴⁹	1.116(9)	-0.5
17 Nucletron, mHDR-v2(361.1)	1.1090 ^{c,e}	1.109	0.0	1.107(8) ^{50,d}	1.109(12)	0.2
18 Nucletron, mHDR-v2r(360.5) ^f	1.1092	-	-	1.1121(8) ^{50,d}	-	-
19 Oncology system, M19(361.0)	1.1103	1.114	-0.3	1.130(3) ⁵¹	-	-
20 Varian, GammaMed 12i(360.5)	1.1103	1.117	-0.6	1.118(3) ⁴⁶	1.118(3)	-0.7
21 Varian, GammaMed Plus(360.5)	1.1100	1.115	-0.4	1.110(1) ⁵²	1.117(5)	-0.6
22 Varian, VariSource(357.7)	1.0378	1.042	-0.4	1.043(5) ⁵³	-	-
23 Varian, VS2000(357.7)	1.0984	1.099	-0.1	1.101(6) ⁵⁴	1.100(6)	-0.1

^a Value calculated using TL estimator. Value including electron transport is 1.1115(17), *i.e.*, (0.12 \pm 0.15)% higher

^b Value is averaged over 5 different Monte Carlo codes³³

^c There is a change in the model of the source described in the database

^d Value is averaged over 3 different Monte Carlo codes⁵⁰

^e Value calculated using TL estimator. Value including electron transport is 1.1077(12), *i.e.*, (0.12 \pm 0.11)% lower.

^f Elekta sells this source as mHDR-v2 and no longer sells the original mHDR-v1.

Table 2: Same as Table 1, except for ^{169}Yb HDR, ^{137}Cs LDR, and ^{60}Co HDR sources.

Source model ($\bar{E}_\gamma/\text{keV}$)	Dose-rate constant, DRC or Λ ($\text{cGy h}^{-1} \text{U}^{-1}$)				
	This work(eb)	Other MC	% Δ (eb,Other)	TG43 _{con} ⁸	% Δ (eb,TG43 _{con})
^{169}Yb HDR					
24 Implant Sciences, 4140 (117.07) ^a	1.1871 ^{b,c}	1.19(3) ⁵⁵	-	-	-
^{137}Cs LDR					
25 BEBIG, CSM11(647.64)	1.0956 ^d	1.096(2) ⁵⁶	-0.03	1.094(18)	0.1
26 Amersham, CDC-1(646.34)	1.1040	1.113(3) ⁵⁷	-0.8	-	-
27 Amersham, CDC-3(647.46)	1.0959	1.103(3) ⁵⁷	-0.6	-	-
28 Walstam, CDC-k4(643.74)	1.0949	1.092(1) ⁵⁸	-	-	-
29 IPL,67-6520(646.3)	0.9505	0.948(26) ⁵⁹	0.3	0.948(3)	0.3
^{60}Co HDR					
30 BEBIG, Co0.A86 (1240.48)	1.0985 ^e	1.094(3) ⁶⁰	0.4	1.092(5)	0.6
31 BEBIG, GK60M21 (1239)	1.0966 ^e	1.093(2) ⁶⁰	0.3	1.089(5)	0.7
32 Shimadzu, Ralston type 1(1210.4)	0.8822 ^e	0.878(4) ⁶¹	0.5	-	-
33 Shimadzu, Ralston type 2 (1211.22)	1.1077 ^e	1.101(5) ⁶¹	0.6	-	-

^a The BD^{10,38} and % Δ (eb, BD) values are 1.186 and 0.09%, respectively^b Value calculated using TL estimator. Value including electron transport is 1.1874(8), *i.e.*, 0.03% larger^c Value is for PCUT = 10 keV. Value for PCUT = 1 keV is 1.1541(4), *i.e.*, 2.8% lower^d Value calculated using TL estimator. Value including electron transport is 1.0990(12), *i.e.*, 0.31% larger^e Values calculated using electron transport. Corresponding values using TL estimator are 1.0845(2) (Co.A86, 1.3% lower), 1.0855(2) (GK60M21, 1.0% lower), 0.8742(2) (Ralston type 1, 0.9% lower), and 1.0947(2) (Ralston type 2, 1.2% lower), respectively

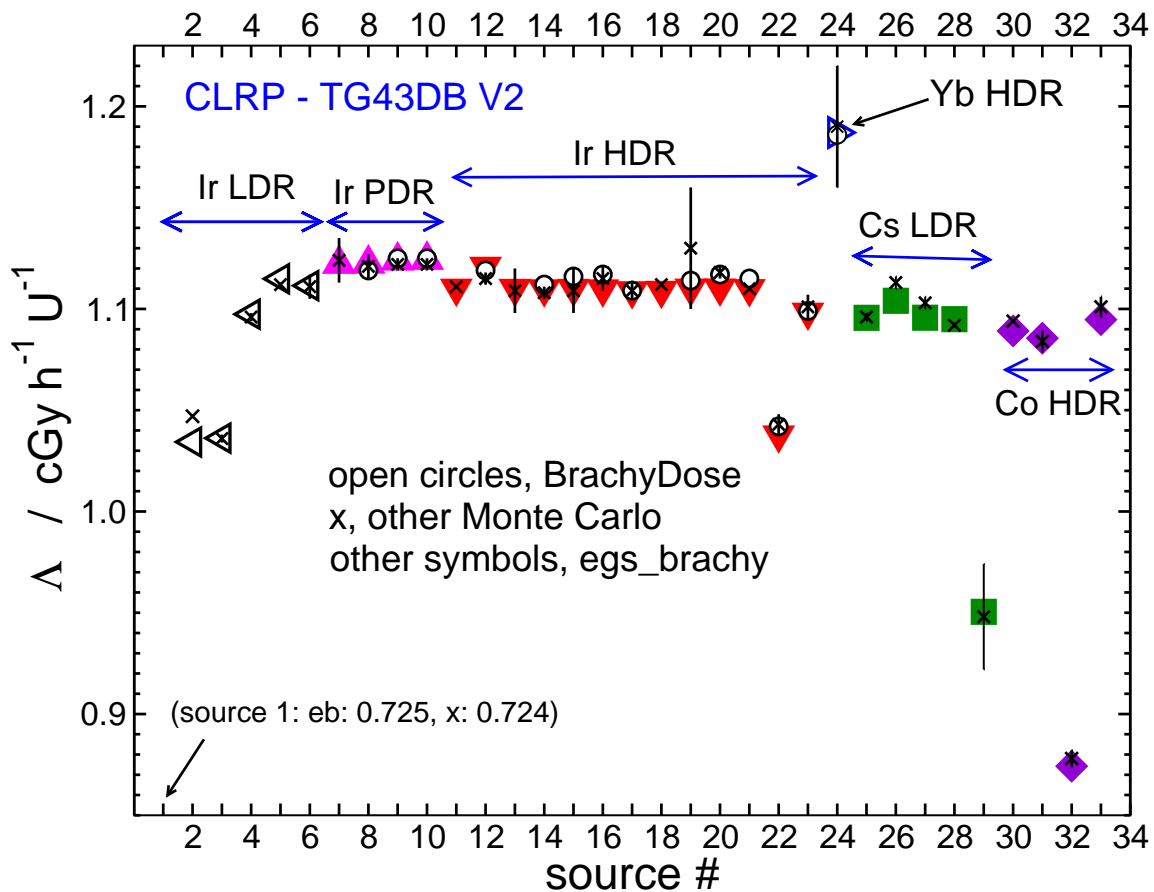


Figure 9: `egs_brachy` calculated values of dose-rate constants, Λ , are shown as: black left triangles for ^{192}Ir LDR, magenta up triangles for ^{192}Ir PDR, red down triangles for ^{192}Ir HDR, a blue right triangle for ^{169}Yb HDR, green squares for ^{137}Cs LDR, and violet diamonds for ^{60}Co HDR sources. Values calculated previously with BrachyDose are open black circles.^{10,38} DRCs from other MC codes with their uncertainties are shown as black x symbols. The statistical uncertainties on `egs_brachy` and BrachyDose values are smaller than their symbols. The x-axis source numbers are in Tables 1 and 2.

TG-229⁸ recommended consensus DRC values for HE sources based on MC values. The last column of Tables 1 and 2 indicate good agreement between the `egs_brachy` results and the consensus values. The mean difference between `CLRP_TG43v2` and `TG-43con` DRC values for different source types are: LDR, 0.2%; PDR and HDR ^{192}Ir , -0.01%; LDR ^{137}Cs , -0.02%; and HDR ^{60}Co , 0.6%: *i.e.*, agreement is excellent where comparisons are available. Overall, $g_L(r)$ and $F(r, \theta)$ values generated from the `egs_brachy` data are in good agreement with the BrachyDose results within statistical uncertainties for all sources studied by both. As discussed previously,¹⁵ significant discrepancies in the calculated doses occurred for some regions very close to the source since BrachyDose did not properly account for statistical uncertainties in the source volume correction whereas these are now properly handled in

egs_brachy.

II.F. Trends seen in the data

In general, for ^{192}Ir sources, as the source length increases above the common 3 to 4 mm range, the DRC values decrease (LDR sources 1-4, HDR sources 22, 23) with the smallest DRC of 0.7245 being for the 3 cm long LDR ^{192}Ir Amersham source (source 1, Table 1 and Figure 9). This is due to the increase in the mean photon pathlength from the source to the reference point at (1 cm, 90°). This leads to increased attenuation in the water phantom but not in vacuum for the S_K geometry and hence the lower DRC. The same applies for the relatively long ^{137}Cs IPL source (source 29, Table 2 and Figure 9) which has the smallest DRC of the ^{137}Cs sources.

The highest DRC among all the HE and LE sources belongs to the ^{169}Yb source with the lowest mean energy of the HE sources (117.1 keV). At these energies there is far more scatter at 1 cm than for higher energy sources. At the reference position, (1 cm, 90°), 33% of the dose is from scattered photons whereas for the source with the next highest DRC (source 12) only 10.5% of the dose at (1 cm, 90°) is from scattered photons. The large amount of scattered dose also leads to ^{169}Yb 's very large $g(r)$ value for r values near 5 cm (see discussion below re Fig 10).

Among the ^{60}Co sources the lowest DRC value is for the Shimadzu Ralston type 1 model (source 32). This is due to the source geometry (Figure 1) in which two symmetric active pellets are spaced by 9 mm of stainless steel which makes it effectively a long source with a low DRC. The lack of radioactivity near the centre of the source leads to an unusual $g(r)$ which reaches a high value near $r=3$ cm but this is due to the low relative dose rate at 1 cm and not excessive scatter as observed with the ^{169}Yb source.

For ^{60}Co sources and some other representative HE sources, DRC values are calculated with electron transport included for the in-phantom calculations rather than using the TL estimator. As mentioned in section II.C.1., the DRCs calculated with electron transport are larger than those with the TL estimator. Differences in DRCs with and without electron transport were $\leq 0.2\%$, 0.2% , 0.12% and 0.3% for the ^{169}Yb (4140), ^{192}Ir (Generic), ^{192}Ir (mHDR-v2) and ^{137}Cs (CSM11) sources, respectively (see footnotes in Tables 1 and 2). For all ^{60}Co source models, the reported DRC includes electron transport. The mean of these DRC values is 1.1% higher than the mean based on the TL estimator (see footnote 'e' in

Table 2).

Figure 10 provides $g_L(r)$ values as a function of r for all 33 HE sources (see section II.C.2. for a discussion of electron transport effects for small radii). For sources of the same radionuclide, $g_L(r > 1 \text{ cm})$ values are very similar except for differences between the Ralston type 1 or type 2 ^{60}Co sources for which the two radioactive pellets are either placed at the source center (class B source) or spaced by a 9 mm Stainless steel rod (class A source).²⁸ The $g_L(r)$ values for the ^{169}Yb source are greater than those for other radionuclides. As discussed above regarding its large DRC (section II.F.), this is because of the large dose from scattered photons which are back and side-scattered for photon energies near 100 keV more than at higher energies. This is seen clearly in the PSS data presented in the database.

The shape of $g_L(r)$ for the ^{60}Co Shimadzu Ralston type 1 source (Figure 1) is distinct from the other sources and matches the expected shape for a class A source.^{15,28} The dose buildup region along the transverse axis of the source is caused by the partial occlusion of the two radioactive pellets by the stainless steel rod at small r values. Also, the geometry factor, $G(r, \theta)$, assumes there is radioactivity near $r=0$ whereas the activity is at least 4.5 mm away.

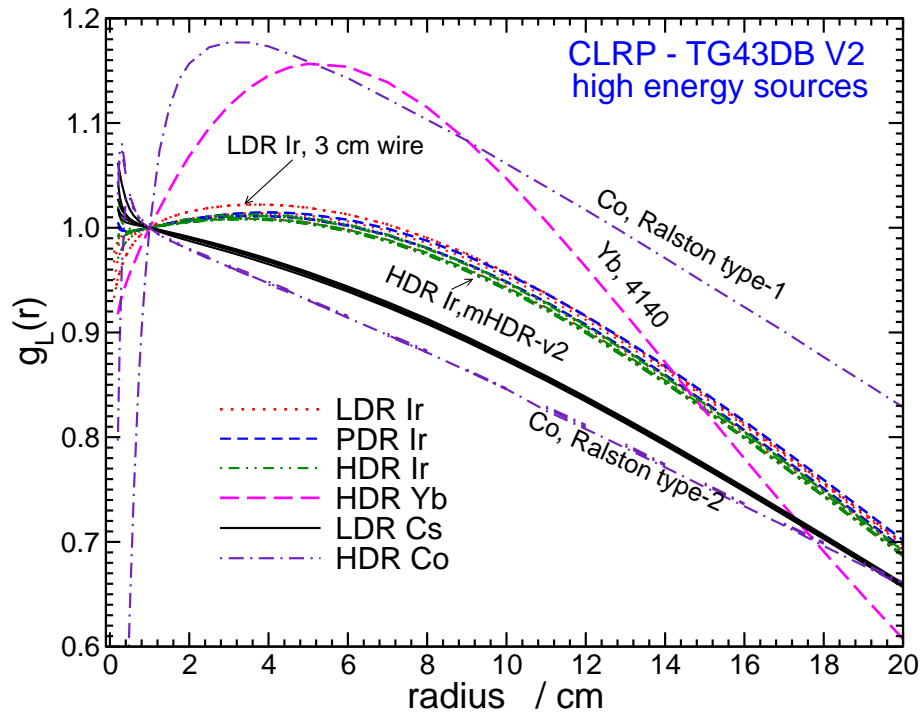


Figure 10: Radial dose functions, $g_L(r)$, of all 33 HE sources including 6 LDR ^{192}Ir (orange dotted lines), 4 PDR ^{192}Ir (blue dashed lines), and 13 HDR ^{192}Ir (green dash-dotted lines), 1 HDR ^{169}Yb (pink dashed lines), 5 LDR ^{137}Cs (nearly identical solid black lines making very thick black line), and 4 HDR ^{60}Co (violet dash-dotted lines). Only ^{60}Co sources used electron transport.

In section II.C.3., the potentially dramatic effects of electron transport on $F(r, \theta)$ values at small radii are pointed out. Here, Figure 11 summarizes $F(1 \text{ cm}, \theta)$ data for all sources in the CLRP_TG43v2 database. In general, in proximal (0°) or distal (180°) regions, anisotropy is increased due to increased attenuation in thicker ends of many source capsules. The most anisotropy is for ^{169}Yb sources and the least anisotropy is for the ^{137}Cs sources, followed by ^{60}Co , and then ^{192}Ir sources.

The ^{60}Co (Ralston type 1) source has a distinctive anisotropy function which, close to 0° or 180° is > 2.5 for $r = 1 \text{ cm}$ since these points are very close to the two active pellets of the source (Figure 1). However at $r = 5 \text{ cm}$ it is similar to other sources with a value near 0.9 (see webpages).

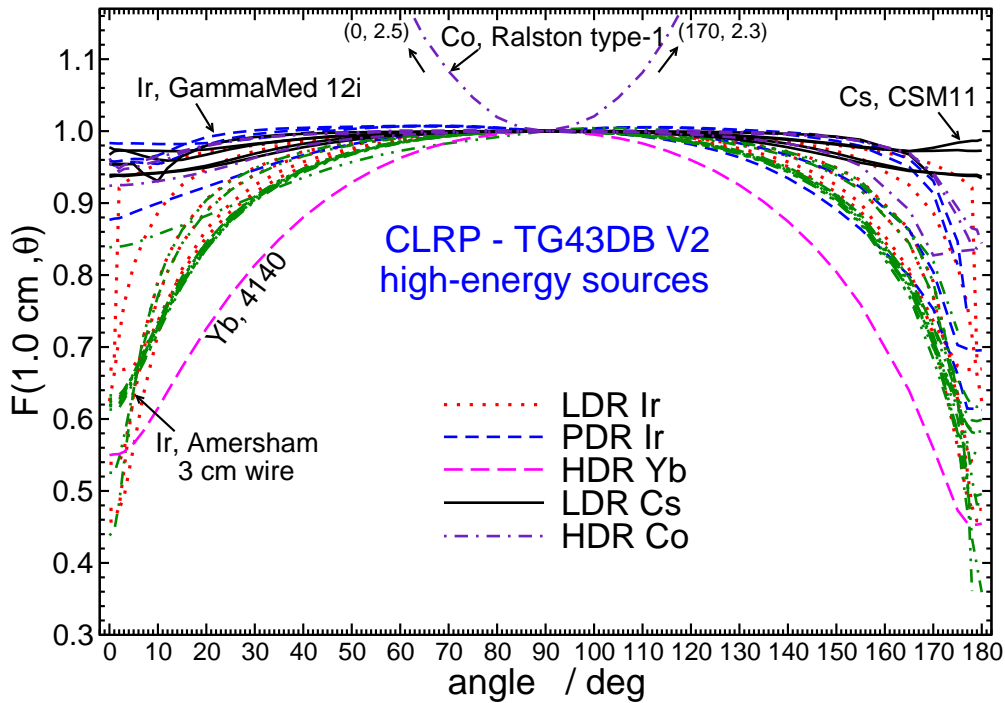


Figure 11: The 2D anisotropy function, $F(1.0 \text{ cm}, \theta)$, of all 33 sources (6 LDR, 4 PDR, and 13 HDR ^{192}Ir , 1 HDR ^{169}Yb , 5 LDR ^{137}Cs , and 4 HDR ^{60}Co) in the HE CLRPv2 database as a function of radionuclides and angle (degrees). Electron transport just included for ^{60}Co sources.

III. Data Format and Access

The CLRP_TG43v2 website is hosted at Carleton University, Ottawa, Canada at https://physics.carleton.ca/clrp/egs_brachy/seed_database_HDRv2 or <http://doi.org/10.22215/clrp/tg43v2>. The main webpage of the database lists the 33 HE and 40 LE brachytherapy sources for which the online datasets are available as well as details about source spectra, half-lives, average energies, voxel resolutions used in MC calculations, and a spreadsheet of S_K^{hist} values as defined just above eqn 1. The database includes all of the same types of data as discussed regarding the LE sources in the CLRP_TG43v2 database and enumerated in our previous database paper.¹⁵ The exception is that for the HE sources, spectra and PSS data are included for all sources rather than just representative sources as done for the LE database.

IV. Potential Impact

Currently most clinical dosimetry of HE sources is based on the TG-43 formalism. The fully benchmarked CLRP_TG43v2 source models developed here will be distributed freely with the `egs_brachy` distribution at https://github.com/clrp-code/egs_brachy for research dosimetry and MC dose calculations in treatment planning or retrospective studies. The PSS data in the database supports the TG-186⁶² recommendations for model-based dose calculations and dose heterogeneity calculations for treatment planning.

The calculated dose-rate constants reported here can be used to support future recommendations for clinical use. They have much better statistical precision than many previous studies. This database may be updated in the future to add dosimetry datasets for new HE sources. In view of the fact that the HE CLRP_TG43v2 values reported here are close to the previous CLRP_TG43v1 data, the most important impact here is validation of the `egs_brachy` source models as well as documentation.

V. Conclusion

The entire LE and HE CLRP_TG43v2 database includes the datasets for 73 sources compared to 44 sources in the CLRP_TG43v1 database, and are available via <http://doi.org/10.22215/clrp/tg43v2>. The CLRP_TG43v2 data are validated in this paper by comparison of `egs_brachy` dose-rate constant data with `BrachyDose` data in CLRP_TG43v1 and any other literature data which exists. Results are in good agreement with previous DRC results. The database also includes extensive comparisons to previous $g(r)$ and $F(r, \theta)$ data. The current work improves statistical uncertainties, source volume corrections, and some source geometry models compared to the CLRP_TG43v1 calculations. It is shown that electron transport must be modelled for ^{60}Co sources although this is not essential for lower-energy sources except very close to the source. The validated `egs_brachy` models of all 33 LE and 44 HE sources will be freely distributed with `egs_brachy` distribution enabling more accurate brachytherapy dosimetry research and advanced model-based dose calculations.

VI. Acknowledgements

This work was supported by the Natural Sciences and Engineering Research Council of Canada, the Canada Research Chairs program, and the Ministry of Research and Innovation of Ontario. The authors thank Harry Allen for assistance running early calculations and Facundo Ballester for providing detailed source dimensions for the BEBIG HDR sources.

References

- ¹ R. Nath, L. L. Anderson, G. Luxton, K. A. Weaver, J. F. Williamson, and A. S. Meigooni, Dosimetry of interstitial brachytherapy sources: Recommendations of the AAPM Radiation Therapy Committee Task Group No. 43, *Med. Phys.* **22**, 209 – 234 (1995).
- ² M. J. Rivard *et al.*, Update of AAPM Task Group No. 43 Report: A revised AAPM protocol for brachytherapy dose calculations, *Med. Phys.* **31**, 633 – 674 (2004).
- ³ M. J. Rivard *et al.*, Erratum: “Update of AAPM Task Group No. 43 Report: A revised AAPM protocol for brachytherapy dose calculations” [*Med. Phys.* **31**, 633–674 (2004)], *Med. Phys.* **31**, 3532 – 3533 (2004).
- ⁴ M. J. Rivard *et al.*, Supplement to the 2004 update of the AAPM Task Group No. 43 Report, *Med. Phys.* **34**, 2187 – 2205 (2007).
- ⁵ M. J. Rivard *et al.*, Supplement 2 for the 2004 update of the AAPM Task Group No. 43 Report: Joint recommendations by the AAPM and GEC-ESTRO, *Med. Phys.* **44**, e297 – e338 (2017).
- ⁶ M. J. Rivard *et al.*, Erratum: “Supplement 2 for the 2004 update of the AAPM Task Group No. 43 Report: Joint recommendations by the AAPM and GEC-ESTRO” [*Med. Phys.* Vol44(9),e297-e338(2017)], *Med. Phys.* **45**, 971 – 974 (2018).
- ⁷ J Perez-Calatayud *et al.*, Dose calculation for photon-emitting brachytherapy sources with average energy higher than 50 keV: Report of the AAPM and ESTRO, *Med. Phys.* **39**, 2904 – 2929 (2012).
- ⁸ J. Perez-Calatayud *et al.*, Dose calculation for photon-emitting brachytherapy sources with average energy higher than 50 keV: Full Report of the AAPM and ESTRO, Report 229, AAPM, Washington, DC, 2012.
- ⁹ R. E. P. Taylor and D. W. O. Rogers, An EGSnrc Monte Carlo-calculated database of TG-43 parameters, *Med. Phys.* **35**, 4228 – 4241 (2008).
- ¹⁰ R. E. P. Taylor and D. W. O. Rogers, EGSnrc Monte Carlo calculated dosimetry parameters for ¹⁹²Ir and ¹⁶⁹Yb brachytherapy sources, *Med. Phys.* **35**, 4933 – 4944 (2008).
- ¹¹ R. E. P. Taylor and D. W. O. Rogers, The Carleton Laboratory for Radiotherapy Physics TG-43 Parameter Database, http://physics.carleton.ca/clrp/seed_database .

- 12 R. E. P. Taylor, G. Yegin, and D. W. O. Rogers, Benchmarking BrachyDose: voxel-based EGSnrc Monte Carlo calculations of TG-43 dosimetry parameters, *Med. Phys.* **34**, 445 – 457 (2007).
- 13 R. M. Thomson and D. W. O. Rogers, Monte Carlo dosimetry for ^{125}I and ^{103}Pd eye plaque brachytherapy with various seed models, *Med. Phys.* **37**, 368 – 376 (2010).
- 14 R. M. Thomson, R. E. P. Taylor, and D. W. O. Rogers, Monte Carlo dosimetry for ^{125}I and ^{103}Pd eye plaque brachytherapy, *Proc. of 54th COMP Annual Scientific Meeting (Canadian Organization of Medical Physicists, Quebec, Quebec)*, 268 – 270 (2008).
- 15 H. Safigholi, M. J. P. Chamberland, R. E. P. Taylor, C. H. Allen, M. P. Martinov, D. W. O. Rogers, and R. M. Thomson, Update of the CLRP TG-43 parameter database for low-energy brachytherapy sources, *Med. Phys.* **47**, 4656 – 4669 (2020).
- 16 M. Chamberland, R. E. P. Taylor, D. W. O. Rogers, and R. M. Thomson, egs_brachy: a versatile and fast Monte Carlo code for brachytherapy, *Phys. Med. Biol.* **61**, 8214 – 8231 (2016).
- 17 I. Kawrakow, E. Mainegra-Hing, F. Tessier, R. Townson, and B. R. B. Walters, The EGSnrc C++ class library, Technical Report PIRS-898(2020), National Research Council Canada, Ottawa, Canada. <http://nrc-cnrc.github.io/EGSnrc/doc/pirs898/index.html>, 2020.
- 18 R. M. Thomson, R. E. P. Taylor, M. J. P. Chamberland, and D. W. O. Rogers, Reply to Comment on 'egs_brachy: a versatile and fast Monte Carlo code for brachytherapy', *Phys. Med. Biol.* **63**, 038002(5pp) (2018).
- 19 I. Kawrakow, E. Mainegra-Hing, D. W. O. Rogers, F. Tessier, and B. R. B. Walters, The EGSnrc code system: Monte Carlo simulation of electron and photon transport, Technical Report PIRS-701, National Research Council Canada, Ottawa, Canada. <http://nrc-cnrc.github.io/EGSnrc/doc/pirs701-egsnrc.pdf>, 2020.
- 20 F. Ballester, D. Granero, J. Pérez-Calatayud, C. S. Melhus, and M. J. Rivard, Evaluation of high-energy brachytherapy source electronic disequilibrium and dose from emitted electrons, *Med. Phys.* **36**, 4250 – 4256 (2009).
- 21 D. W. O. Rogers and R. W. Townson, On calculating kerma, collision kerma and radiative yields, *Med. Phys.* **46**, 5173 – 5184 (2019).
- 22 M. J. Berger and J. H. Hubbell, XCOM: Photon cross sections on a personal computer, Report NBSIR87-3597, National Institute of Standards Technology (NIST), Gaithersburg, MD 20899, U.S.A., 1987.
- 23 ICRU, ICRU Report Committee Activities, in *ICRU News*(ICRU, Bethesda MD), June, 20 (1990).
- 24 L. A. DeWerd *et al.*, A dosimetric uncertainty analysis for photon-emitting brachytherapy sources: Report of AAPM Task Group No. 138 and GEC-ESTRO, *Med. Phys.* **38**, 782 – 801 (2011).
- 25 Brookhaven National Laboratory, National Nuclear Data Center, https://www.nndc.bnl.gov/nudat3/indx_dec.jsp.
- 26 F. Ballester, C. Hernandez, J. Perez-Calatayud, and F. Liso, Monte Carlo calculations of dose rate distributions around ^{192}Ir wires, *Med. Phys.* **24**, 1221–1228 (1997).

- 27 D. W. O. Rogers, Inverse square corrections for FACs and WAFACs, *Appl. Radiat. Isot.* **153**, 108638(8pp) (2019).
- 28 R. E. P. Taylor and D. W. O. Rogers, More accurate fitting of ^{125}I and ^{103}Pd radial dose functions, *Med. Phys.* **35**, 4242 – 4250 (2008).
- 29 E. Mainegra-Hing, D. W. O. Rogers, R. W. Townson, B. R. B. Walters, F. Tessier, and I. Kawrakow, The EGSnrc g application, Technical Report PIRS-3100, National Research Council Canada, Ottawa. <https://nrc-cnrc.github.io/EGSnrc/doc/pirs3100-g-refman.pdf>, 2020.
- 30 J. Borg and D. W. O. Rogers, Spectra and Air-Kerma Strength for Encapsulated ^{192}Ir Sources, *Med. Phys.* **26**, 2441 – 2444 (1999).
- 31 D. Baltas, P. Karaikos, P. Papagiannis, L. Sakelliou, E. Loeffler, and N. Zamboglou, Beta versus gamma dosimetry close to Ir-192 brachytherapy sources, *Med. Phys.* **28**, 1875–1882 (2001).
- 32 R. Wang and X. A. Li, Dose characterization in the near-source region for two high dose rate brachytherapy sources, *Med. Phys.* **29**, 1678–1686 (2002).
- 33 F. Ballester *et al.*, A generic high-dose rate ^{192}Ir brachytherapy source for evaluation of model-based dose calculations beyond the TG-43 formalism, *Med. Phys.* **42**, 3048 – 3062 (2015).
- 34 B. Duchemin and N. Coursol, Reevaluation de l' ^{192}Ir , Technical Note LPRI/93/018, DAMRI, CEA, France (1993).
- 35 J. Borg and D. W. O. Rogers, Monte Carlo Calculations of Photon Spectra in Air from ^{192}Ir Sources, NRC Report PIRS-629r , (35pp)<https://doi.org/10.4224/5764262> (1998).
- 36 Bé, M.-M. *et-al.*, *Table of Radionuclides*, volume 3 of *Monographie BIPM-5*, Bureau International des Poids et Mesures, Pavillon de Breteuil, F-92310 Sèvres, France, 2006.
- 37 ICRU, Dosimetry of External Beta Rays for Radiation Protection, ICRU Report 56, ICRU, Washington D.C., 1997.
- 38 R. E. P. Taylor and D. W. O. Rogers, An EGSnrc Monte Carlo-calculated database of TG-43 parameters, *Med. Phys.* **35**, 4228 – 4241, http://physics.carleton.ca/clrp/seed_database (2008).
- 39 P. Karaikos, P. Papagiannis, A. Angelopoulos, L. Sakelliou, D. Baltas, P. Sandilos, and L. Vlachos, Dosimetry of ^{192}Ir wires for LDR interstitial brachytherapy following the AAPM TG-43 dosimetric formalism, *Med. Phys.* **28**, 156–166 (2001).
- 40 J. Perez-Calatayud, F. Lliso, V. Carmona, F. Ballester, and C. Hernandez, Monte Carlo calculation of dose rate distributions around 0.5 and 0.6 mm in diameter ^{192}Ir wires, *Med. Phys.* **26**, 395–401 (1999).
- 41 R. van der Laarse, G. Granero, J. Perez-Calatayud, A. S. Meigooni, and F. Ballester, Dosimetric characterization of Ir-192 LDR elongated sources, *Med. Phys.* **35**, 1154 – 1161 (2008).
- 42 F. Ballester, D. Granero, J. Perez-Calatayud, E. Casal, and V. Puchades, Monte Carlo dosimetric study of Best Industries and Alpha Omega Ir-192 brachytherapy seeds, *Med. Phys.* **31**, 3298 – 3305 (2004).

- ⁴³ D. Granero, J. Perez-Calatayud, and F. Ballester, Monte Carlo study of the dose rate distributions of the Ir2.A85-2 and Ir2.A85-1 Ir-192 afterloading sources, *Med. Phys.* **35**, 1280 – 1287 (2008).
- ⁴⁴ P. Karaiskos, A. Angelopoulos, E. Pantelis, P. Papagiannis, L. Sakelliou, E. Kouwenhoven, and D. Baltas, Monte Carlo dosimetry of a new ¹⁹²Ir pulsed dose rate brachytherapy source, *Med. Phys.* **30**, 9–16 (2003).
- ⁴⁵ J. Perez-Calatayud, F. Ballester, M. Serrano-Andres, V. Puchades, J. Lluch, Y. Limami, and F. Casal, Dosimetry characteristics of the Plus and 12i Gammamed PDR ¹⁹²Ir sources, *Med. Phys.* **28**, 2576–2585 (2001).
- ⁴⁶ F. Ballester *et al.*, Monte Carlo dosimetry of the Buchler high dose rate 192-Ir source, *Phys. Med. Biol.* **46**, N79–N90 (2001).
- ⁴⁷ D. Granero, J. Perez-Calatayud, and F. Ballester, Monte Carlo calculation of the TG-43 dosimetric parameters of a new BEBIG Ir-192 HDR source, *Radiother. Oncol.* **76**, 79–85 (2005).
- ⁴⁸ D. Granero, J. Perez-Calatayud, E. Casal, , F. Ballester, and J. Venselaar, A dosimetric study on the Ir-192 high dose rate Flexisource, *Med. Phys.* **33**, 4578–4582 (2006).
- ⁴⁹ J. F. Williamson and Z. Li, Monte Carlo aided dosimetry of the microselectron pulsed and high dose-rate ¹⁹²Ir sources, *Med. Phys.* **22**, 809 – 819 (1995).
- ⁵⁰ D. Granero, J. Vijande, F. Ballester, and M. J. Rivard, Dosimetry revisited for the HDR ¹⁹²Ir brachytherapy source model mHDR-v2, *Med. Phys.* **38**, 487–494 (2011).
- ⁵¹ D. C. Medich and J. J. Munro, Monte Carlo characterization of the M-19 high dose rate Iridium-192 brachytherapy source, *Med. Phys.* **34**, 1999–2006 (2007).
- ⁵² J. Wu, Y. Xie, Z. Ding, F. Li, and L. Wang, Monte Carlo study of TG-43 dosimetry parameters of GammaMed Plus high dose rate ¹⁹²Ir brachytherapy source using TOPAS, *J of App Clin Med Phys* **22**, 146–153 (2021).
- ⁵³ P. Karaiskos, A. Angelopoulos, P. Baras, L. Sakelliou, P. Sandilos, K. Dardoufas, and L. Vlachos, A Monte Carlo investigation of the dosimetric characteristics of the VariSource ¹⁹²Ir high dose rate brachytherapy source, *Med. Phys.* **27**, 1498–1592 (2000).
- ⁵⁴ A. Angelopoulos, P. Baras, L. Sakelliou, P. Karaiskos, and P. Sandilos, Monte Carlo dosimetry of a new ¹⁹²Ir high dose rate brachytherapy source, *Med. Phys.* **27**, 2521–2527 (2000).
- ⁵⁵ D. Medich, M. Tries, and J. Munro, Monte Carlo characterization of an ytterbium-169 high dose rate brachytherapy source with analysis of statistical uncertainty, *Med. Phys.* **33**, 163–172 (2006).
- ⁵⁶ F. Ballester, J. L. Lluch, Y. Limami, M. A. Serrano, E. Casal, J. Perez-Calatayud, and F. Lliso, A Monte Carlo investigation of the dosimetric characteristics of the CSM11 ¹³⁷Cs source from CIS, *Med. Phys.* **27**, 2182–2189 (2000).
- ⁵⁷ J. Perez-Calatayud, F. Ballester, M. A. Serrano-Andrés, J. L. Lluch, V. Puchades, Y. Limami, and E. Casal, Dosimetric characteristics of the CDC-type miniature cylindrical ¹³⁷Cs brachytherapy sources, *Med. Phys.* **29**, 538–543 (2002).

- ⁵⁸ J. Perez-Calatayud, F. Ballester, J. L. Lluch, M. A. Serrano-Andrés, E. Casal, V. Puchades, and Y. Limami, Monte Carlo calculation of dose rate distributions around the Walstam CDC.K-type ^{137}Cs sources, *Phys. Med. Biol.* **46**, 2029–2040 (2001).
- ⁵⁹ A. S. Meigooni, C. Wright, R. A. Koon, S. B. Awan, D. Granero, J. Perez-Calatayud, and F. Ballester, TG-43 U1 based dosimetric characterization of model 67-6520 Cs-137 brachytherapy source, *Med. Phys.* **36**, 4711 – 4719 (2009).
- ⁶⁰ T. P. Selvam and S. Bhola, Technical Note: EGSnrc-based dosimetric study of the BEBIG Co-60 HDR brachytherapy sources, *Med. Phys.* **37**, 1365 – 1370 (2010).
- ⁶¹ P. Papagiannis, A. Angelopoulos, E. Pantelis, L. Sakelliou, P. Karaiskos, and Y. Shimizu), Monte Carlo dosimetry of ^{60}Co HDR brachytherapy sources, *Med. Phys.* **30**, 712–721 (2003).
- ⁶² L. Beaulieu *et al.*, Report of the Task Group 186 on model-based dose calculation methods in brachytherapy beyond the TG-43 formalism: Current status and recommendations for clinical implementation, *Med. Phys.* **39**, 6208 – 6236 (2012).